Quantum fluctuations driven orientational disordering: A finite-size scaling study

R. Martoňák,[1,2,*] D. Marx,[3] and P. Nielaba[1]
[1]*Institut für Physik, KoMa 331, Johannes Gutenberg-Universität, Staudingerweg 7, 55099 Mainz, Germany*
[2]*Max-Planck-Institut für Polymerforschung, Ackermannweg 10, 55021 Mainz, Germany*
[3]*Max-Planck-Institut für Festkörperforschung, Heisenbergstrasse 1, 70569 Stuttgart, Germany*
(Received 20 August 1996)

The orientational ordering transition is investigated in the quantum generalization of the anisotropic-planar-rotor model in the low-temperature regime. The phase diagram of the model is first analyzed within the mean-field approximation. This predicts at $T=0$ a phase transition from the ordered to the disordered phase when the strength of quantum fluctuations, characterized by the rotational constant Θ, exceeds a critical value Θ_c^{MF}. As a function of temperature, mean-field theory predicts a range of values of Θ where the system develops long-range order upon cooling, but enters again into a disordered state at sufficiently low temperatures (reentrance). The model is further studied by means of path-integral Monte Carlo simulations in combination with finite-size scaling techniques, concentrating on the region of parameter space where reentrance is predicted to occur. The phase diagram determined from the simulations does not seem to exhibit reentrant behavior; at intermediate temperatures a pronounced increase of short-range order is observed rather than a genuine long-range order. [S1063-651X(97)04802-2]

PACS number(s): 05.70.Fh, 05.30.−d, 64.60.Cn, 68.35.Rh

I. MOTIVATION

Physisorbates are experimental realizations of quasi-two-dimensional systems that display an extremely rich phase behavior due to the competition between intermolecular and molecule-surface interactions, as documented, e.g., in Refs. [1–5]. Correspondingly, there is a wealth of phase transitions between the various ordered phases as a function of temperature and coverage. Since many of these transitions occur at fairly low temperatures, quantum effects might play an important or even crucial role [3,4], as recently demonstrated for the ordering of hydrogen isotopes on graphite [6]. Molecular systems are particularly interesting as they possess orientational degrees of freedom that can order in addition to the positions [5]. In the case of linear molecules, the anisotropic-planar-rotor (APR) model [7,8] was devised to describe the herringbone (quadrupolar orientational two-sublattice) ordering transition [5], e.g., in commensurate N_2 monolayers on graphite. The classical two-dimensional APR model consists of planar rotators pinned with their center of rotation on a triangular lattice and interacting via nearest-neighbor quadrupolar interactions only; a three-dimensional version has also been proposed and investigated in various approximations [9].

Over the years the APR Hamiltonian acquired the status of a statistical-mechanical *model* in its own right; see Refs. [10,5]. Many of these activities arose because the order of the APR phase transition turned out to be extremely challenging to determine [11], finally favoring a first-order phase transition that is ''weak'' and fluctuation driven [12]; see the detailed review in Ref. [5]. The plain APR model was generalized to include vacancies or impurities [13–15], as well as multipole interactions other than those of quadrupolar symmetry [14,16]. Simplified Hamiltonians were obtained after discretizing the continuous rotations to an anisotropic six-state model [17] or to more general discrete models [18]. We introduced quantum generalizations of interacting two-dimensional quadrupolar lattice systems [19,20], in particular of the APR model [21,22]. For a given lattice, the classical APR model has no free parameter because the quadrupolar coupling constant K only sets the energy scale of the model. Correspondingly, the phase diagram is one dimensional and is fully characterized by a single number, the transition temperature scaled by the constant K. In the quantum case, however, the quantum kinetic energy is determined by the mechanical moment of inertia I associated with the angular motion of the two-dimensional rotators. The resulting rotational constant $\Theta=\hbar^2/2I$ is an additional independent parameter that determines the strength and energy scale of the quantum fluctuations, and in the limit $\Theta\to 0$ the quantum APR model reduces to the classical one. The resulting behavior of the quantum APR model is governed by the interplay between thermal and quantum fluctuations. This interesting feature is present also in other systems, such as Ising models in transverse field [23,24], models for granular superconductors [25] and superconducting arrays [26], lattice ϕ^4 theory [27], and quantum four-state clock models [28]; see Ref. [22] for a short discussion of these related models.

In our previous studies [21,22] we presented an initial *qualitative* exploration of the two-dimensional (2D) quantum APR Hamiltonian, using path-integral Monte Carlo (PIMC) simulations [29] adapted to rotational motion restricted to two dimensions [30]. It was demonstrated numerically [22] that low-order approximation schemes such as quasiclassical Monte Carlo simulations using the quadratic Feynman-Hibbs effective potential, and the simple quasiharmonic approximation are useful only in the regime of small rotational constants $\Theta\to 0$, whereas they fail completely in the large-Θ range that is of interest here. The phase boundaries were

*Permanent address: Department of Physics, Faculty of Electrical Engineering, Slovak Technical University, Ilkovičova 3, 812 19 Bratislava, Slovakia.

estimated phenomenologically from the behavior of the order parameter, i.e., without applying any kind of finite-size scaling to the data obtained from $30^2=900$ interacting rotators. Increasing the value of Θ, four distinct regimes were found based on the shape of the orientational order parameter. For small Θ, the transition temperature and value of the ground-state order parameter obtained from the classical model get renormalized just to smaller values. In the opposite limit of large Θ, the quantum fluctuations are that strong that they do not allow for any ordering even in the ground state. More interesting are the intermediate regimes. For increasing Θ a crossover was found where there is residual ground-state order, although significantly depressed from its classical value, but the order parameter inside the ordered phase first *increases* upon heating and goes through a maximum at some intermediate temperature before it decays in the disordered phase. For even larger Θ, there seemed to be a region in parameter space with vanishing ground-state order together with residual order at finite temperatures. The ''tentative and qualitative phase diagram'' in the Θ-T plane thus seemed to exhibit a *reentrance* phenomenon in a range of Θ where quantum and thermal fluctuations are competitive; see Fig. 9 in Ref. [22]. A similar behavior was already discovered in mean-field studies of certain quantum Ising models [24], quantum four-state clock models with quadrupolar interactions [28], and interacting 3D quadrupolar rotators [31]. The reentrance in the two-level systems was also found to be present when fluctuations were included to lowest order in the form of a Kirkwood correction on top of the Bragg-Williams expressions [24]. The reentrance in the three-dimensional system was ascribed in Ref. [31] to two distinct first-order phase transitions, a standard order-disorder transition at higher temperatures that is also present in the corresponding classical model, and a transition of pure quantum nature at low temperatures.

With the present paper, we concentrate on the region of the phase diagram of the 2D quantum APR model where reentrance might be expected to occur. We use first a mean-field approximation and then a PIMC simulation. The aim of the work is to study the orientational transition behavior in the reentrance regime. In particular, we are interested to find out whether there are actually two distinct *phase transitions* occurring as a function of temperature. To this end, we simulate the system on several length scales and use finite-size scaling, in particular Binder's cumulant [32,33], to analyze the order parameter distributions.

The main body of the paper is organized as follows. The quantum APR model together with its order parameter is defined in Sec. II. In Sec. III A, the quantum PIMC simulation technique is described, followed by the definition of the relevant observables in Sec. III B and an outline of the finite-size scaling analysis method in Sec. III C. The mean-field approximation is worked out in Sec. IV. In Sec. V, the results of the simulation are discussed and compared with those of the mean-field approximation and a possible scenario is suggested. In Sec. VI, we summarize the results and draw some conclusions.

II. QUANTUM ANISOTROPIC-PLANAR-ROTOR MODEL

The subjects of this study are the properties and in particular the phase diagram of the quantum-mechanical version of the APR model [7,8]. The classical APR Hamiltonian was extensively studied over the years, both numerically and analytically; see Ref. [5], where the properties of the classical model including the order parameter and the herringbone orientationally ordered ground state are discussed. The N quadrupolar rotators are fixed with their center of mass on an ideal rigid triangular lattice $\{\mathbf{R}_j\}$ and only rotations in the two-dimensional surface plane are allowed. The interactions are truncated at the first-neighbor shell and the rotators interact exclusively with their six nearest neighbors via the anisotropic part of a quadrupole-quadrupole potential of strength K in two dimensions. The quantum generalization results after supplementing this classical Hamiltonian with a noncommuting angular momentum part $[L_j,\varphi_i]=-i\hbar\delta_{j,i}$ which introduces quantum dispersion and thus qualitatively different effects due to additional fluctuations and tunneling. Correspondingly, the quantum APR Hamiltonian reads

$$H=\sum_{j=1}^{N}\frac{L_j^2}{2I}+\sum_{\langle j,i\rangle}^{N}V(\varphi_j,\varphi_i) \tag{2.1}$$

$$=-\Theta\sum_{j=1}^{N}\frac{\partial^2}{\partial\varphi_j{}^2}+K\sum_{\langle j,i\rangle}^{N}\cos(2\varphi_j+2\varphi_i-4\phi_{j,i}), \tag{2.2}$$

where the angle φ_j of the jth rotator pinned at site $\mathbf{R}_j$ is defined relative to one symmetry axis of the triangular lattice and the six phases $\phi_{j,i}$ measure the angle between neighboring sites $\mathbf{R}_j$ and $\mathbf{R}_i$ on this lattice, i.e., $\phi_{j,i}\in\{0,\pi/3,2\pi/3,\pi,4\pi/3,5\pi/3\}$. We stress that for this system the triangular lattice structure is essential in order to produce a nontrivial ordered phase. On a simple square lattice the quadrupolar interaction would just favor unfrustrated perpendicular nearest-neighbor orientations of the characteristic T shape.

The moment of inertia I determines the rotational constant $\Theta=\hbar^2/2I$, which is the parameter that controls the strength of quantum effects. The other parameter of the model, which is the quadrupolar coupling constant K, can be conveniently taken as the energy and temperature scale. We can thus reduce all quantities related to energies by K and define, e.g., the dimensionless temperature $T^*=k_BT/K$, energy $E^*=E/K$, and rotational constant $\Theta^*=\Theta/K$.

The long-range order parameter sensitive to herringbone ordering of the rotational axis has three ($\alpha=1,2,3$) *independent* components

$$\Phi_\alpha=\frac{1}{N}\sum_{j=1}^{N}\sin(2\varphi_j-2\eta_\alpha)\exp[i\mathbf{Q}_\alpha\cdot\mathbf{R}_j], \tag{2.3}$$

where

$$\mathbf{Q}_1=\pi(0,2/\sqrt{3}),\quad \eta_1=0,$$

$$\mathbf{Q}_2=\pi(-1,-1/\sqrt{3}),\quad \eta_2=2\pi/3,$$

$$\mathbf{Q}_3=\pi(1,-1/\sqrt{3}),\quad \eta_3=4\pi/3. \tag{2.4}$$

III. NUMERICAL METHODS

A. Path-integral Monte Carlo simulation technique

We study the properties of the Hamiltonian (2.2) by means of PIMC simulations; for general reviews on the concept of PIMC we refer to Ref. [29]. We just stress here that for rotational motion in two dimensions different features connected to the restricted integration space show up in the formalism [34]. This latter aspect and our implementation of these specialties in a PIMC scheme is discussed in detail in Ref. [19], and here we present only the essential features.

In general, the partition function of a Hamiltonian of type (2.1) is given by

$$Z = \mathrm{Tr}\exp[-\beta H] \tag{3.1}$$

$$\begin{aligned} &= \lim_{P\to\infty}\left(\frac{IP}{2\pi\hbar^2\beta}\right)^{NP/2} \\ &\times\prod_{j=1}^{N}\left\{\sum_{n_j=-\infty}^{\infty}\int_0^{2\pi}d\varphi_j^{(1)}\prod_{s=2}^{P}\left[\int_{-\infty}^{\infty}d\varphi_j^{(s)}\right]\right\} \\ &\times\exp\left\{-\beta\sum_{s=1}^{P}\left[\sum_{j=1}^{N}\frac{IP}{2\hbar^2\beta^2}[\varphi_j^{(s)}-\varphi_j^{(s+1)}+2n_j\pi\delta_{s,P}]^2\right.\right. \\ &\left.\left.+\sum_{\langle j,i\rangle}^{N}\frac{1}{P}V(\varphi_j^{(s)},\varphi_i^{(s)})\right]\right\}, \end{aligned} \tag{3.2}$$

where $V(\varphi_j^{(s)},\varphi_i^{(s)})$ denotes the APR pair potential of Eq. (2.2) evaluated separately for the configuration at each imaginary time slice $s=1,\ldots,P$. Each quantum-mechanical rotational degree of freedom is represented in this path-integral representation by P classical rotators that form closed loops and interact via harmonic-type interactions; for the related ring-polymer picture see Refs. [35,29]. The parameter P is the Trotter number, the configuration $\{\varphi_j^{(1)},\varphi_j^{(2)},\ldots,\varphi_j^{(P)}\}$ is a realization of a Trotter path, and the path integral results from the proper integration and summation over all possible paths. However, contrary to path integrals for translational degrees of freedom, these loops do not need to be closed using periodic boundary conditions, but only mod 2π; note that the classical angles $\varphi_j^{(s)}$ of Eq. (3.2) are not confined to $[0,2\pi)$ but are allowed on the whole interval $[-\infty,\infty]$. The resulting mismatch n_j is called the ''winding number'' of the jth path [34] and the formulation (3.2) is the ''winding number representation'' of the partition function. Only the Boltzmann-weighted summation over all possible winding numbers in addition to the integration over all paths having a certain winding number yields the correct quantum partition function in the Trotter limit $P\to\infty$; see Ref. [19] for a full discussion of that issue. Thus we have to include in the algorithm, in addition to local and global moves of the angular degrees of freedom $\{\varphi_j^{(s)}\}$, also attempts to change the winding numbers $\{n_j\}$ of the individual rotators. Our algorithm was tested [30,19] against exact (single-particle) results and a close agreement was observed. In a previous study [22] it turned out that the use of a finite Trotter number of $P=500$ at a temperature of $T^*=0.03$ and a progressive linear decrease of P with increasing temperature were sufficient to be in the large-P limit as required in Eq. (3.2). We note that other methods have been suggested for the path-integral simulation of rotational degrees of freedom in two-dimensional [36] and three-dimensional space [37], respectively.

In the present paper we study in particular finite-size effects on the quantum APR transition. The required different linear dimensions L of the system were chosen to range from $N=L^2=144$ to 900, where additional data from Ref. [22] have been included in the analysis. We equilibrated the systems starting from the ideally ordered herringbone ground state and made, where possible, use of previous runs either at lower temperatures or smaller rotational constant. Our statistics is based on the order of 10^5 PIMC steps for each data point; a typical CPU time per data point was of the order of 50 h on a CRAY-YMP supercomputer.

B. Observables and estimators

The quantities we determined from the simulations are the kinetic and the potential energy, order parameter, quantum librational amplitudes, as well as fourth-order (3.11) and second-order (3.12) cumulants.

The energies were obtained from the primitive estimator [29], which proved to be sufficient in the present case [19]. The kinetic energy E_{kin} and the potential energy E_{pot} per particle are given by

$$E_{\mathrm{kin}} = \frac{Pk_BT}{2} - \left\langle \frac{1}{N}\sum_{j=1}^{N}\sum_{s=1}^{P}\frac{IP}{2\hbar^2\beta^2} \times[\varphi_j^{(s)}-\varphi_j^{(s+1)}+2n_j\pi\delta_{s,P}]^2\right\rangle, \tag{3.3}$$

$$E_{\mathrm{pot}} = \left\langle \frac{1}{P}\sum_{s=1}^{P}\frac{1}{N}\sum_{\langle j,i\rangle}^{N}V(\varphi_j^{(s)},\varphi_i^{(s)})\right\rangle, \tag{3.4}$$

and the total energy E_{tot} is given by the sum of E_{kin} and E_{pot}. The estimator for the order parameter component Φ_α is given by the expression

$$\Phi_\alpha = \frac{1}{NP}\sum_{j=1}^{N}\sum_{s=1}^{P}\sin(2\varphi_j^{(s)}-2\eta_\alpha)\exp[i\mathbf{Q}_\alpha\cdot\mathbf{R}_j], \tag{3.5}$$

which trivially follows from Eq. (2.3). In the following we will use the total long-range order parameter defined as the length [19,12]

$$\Phi = \left\langle\left[\sum_{\alpha=1}^{3}\Phi_\alpha^2\right]^{1/2}\right\rangle \tag{3.6}$$

of the three component vector order parameter (3.5).

A quantity that measures the quantum delocalization of the rotational degrees of freedom can be defined by the expression [19]

$$R_\varphi = \left\langle\frac{1}{N}\sum_{j=1}^{N}\frac{1}{P}\sum_{s=1}^{P}\left[\varphi_j^{(s)}-\frac{1}{P}\sum_{k=1}^{P}\varphi_j^{(k)}\right]^2\right\rangle^{1/2}. \tag{3.7}$$

This average spread is by its definition zero for a classical system and is thus a measure of the pure quantum contribution to the librations or rotations of the individual rotators.

C. Finite-size scaling

An identifying characteristic of a continuous phase transition is the divergence of the correlation length ξ at the critical temperature T_c, with $\xi \sim |t|^{-\nu}$ for $t := 1 - T/T_c$, $|t| \ll 1$. Under these conditions on the reduced distance from the phase transition $t \geqslant 0$, the order parameter Φ in the infinitely large system depends on t as $\Phi \sim |t|^{\beta}$, where ν and β denote here the usual critical exponents. In finite systems of linear dimension L the order parameter is given by the expression [33]

$$\langle \Phi \rangle_L = L^{-\beta/\nu} \widetilde{\Phi}(L/\xi), \tag{3.8}$$

where $\widetilde{\Phi}$ is the scaling function that is associated to Φ. The order parameter distribution function $P_L(\Phi)$ in the finite system is thus a function of the scaling variables $L^{\beta/\nu}\Phi$ and L/ξ,

$$P_L(\Phi) = L^{\beta/\nu} \widetilde{P}(L^{\beta/\nu}\Phi, L/\xi), \tag{3.9}$$

and the kth moment of the order parameter distribution function is given by

$$\langle \Phi^k \rangle_L = L^{\beta/\nu} \int d\Phi \ \Phi^k \widetilde{P}(L^{\beta/\nu}\Phi, L/\xi) = L^{-\beta k/\nu} \widetilde{\Phi}_k(L/\xi), \tag{3.10}$$

where $\langle \rangle_L$ denote the canonical average of a system of linear dimension L.

A very useful quantity for the determination of a critical point that is directly based on order parameter moments is the fourth-order cumulant [32,33] $U_L^{(4)}$ or the second-order cumulant [38] $U_L^{(2)}$ defined as

$$U_L^{(4)} = 1 - \frac{\langle \Phi^4 \rangle_L}{3 \langle \Phi^2 \rangle_L^2}, \tag{3.11}$$

$$U_L^{(2)} = 1 - \frac{\langle \Phi^2 \rangle_L}{3 \langle \Phi \rangle_L^2}, \tag{3.12}$$

where one can see that the explicit dependence on system size drops out if the kth moments $\sim L^{-\beta k/\nu}$ are reexpressed with the aid of Eq. (3.10) in terms of their scaling functions. We compile here only the main features and usage of these quantities and refer for further details to the literature [32,33].

In the case of second-order transitions, the cumulants adopt a nontrivial universal value U^* at the critical point, irrespective of system sizes $\{L\}$ in the scaling limit. Thus, plotting $U_L^{(4)}(T)$ or $U_L^{(2)}(T)$ for different linear dimensions as a function of temperature yields an intersection point $U(T_c) =: U^*$, which gives an accurate estimate of the critical temperature in the *infinite* system for a temperature-driven second-order transition. Below and above the transition, the cumulants flow to trivial limiting values depending on the definition of the order parameter; the larger the system, the faster the convergence. Instead of the temperature, other parametrizations of approaching a critical point can also be chosen. More recently, it was worked out that the concept of order parameter cumulant crossings is also useful to analyze first-order phase transitions [39]. In this case, one can observe an *effective* crossing point at a nonuniversal value U^* at the phase transition. The approach of both the transition point and the value of U at the transition to the infinite system limit is quite fast: the correction depends, roughly speaking, on the inverse volume of the system [39]. Thus, for practical numerical purposes the order parameter cumulant can be taken as acquiring an intersection point at a first-order transition in a way similar to that occurring at a second-order transition.

IV. MEAN-FIELD THEORY

In this section we start from the Hamiltonian (2.2) and determine the phase diagram for our model using a mean-field approximation. This consists of considering a single quantum rotator in the mean field of its six nearest neighbors and finding a self-consistent condition for the order parameter. Solving the latter condition, we determine the phase boundary and also the order of the transition. Our mean-field approximation is similar in spirit to that used in Ref. [31] for the case of 3D rotators.

We shall assume that the order parameter component Φ_1 becomes nonzero in the ordered phase, $\Phi_1 = \pm \langle \sin 2\varphi \rangle \neq 0$ [we choose a positive sign for the single rotator, note that the sign alternates passing from one row of the herringbone structure to another, see Eq. (2.3)], while $\Phi_2 = \Phi_3 = 0$. Now it is useful for a moment to return to normal (nonreduced) units for Θ, K, and T. In order to proceed, we write each interaction term $K\cos(2\varphi + 2\varphi' - 4\phi_{ij})$ as a product of trigonometric functions depending separately on the angular variables φ of the single rotator and φ' of its nearest neighbors. Averaging over the variables φ', we find the following contributions: for the two terms corresponding to $\phi_{ij} = 0$ we get $-2K\Phi_1 \sin 2\varphi$, for the two terms corresponding to $\phi_{ij} = \pi/3$ we get $-K\Phi_1 \sin 2\varphi + \sqrt{3}K\Phi_1 \cos 2\varphi$ and for the two terms corresponding to $\phi_{ij} = 2\pi/3$ we get $-K\Phi_1 \sin 2\varphi - \sqrt{3}K\Phi_1 \cos 2\varphi$. Summing these contributions from all six nearest neighbors, we find the total mean-field potential acting on the single rotator, which reads

$$H_{\rm pot}^{\rm MF} = -4K\Phi_1 \sin 2\varphi. \tag{4.1}$$

Adding the kinetic energy, we get the corresponding one-particle Schrödinger equation for the on-site problem

$$H^{\rm MF}\Psi = \left(-\Theta \frac{d^2}{d\varphi^2} - 4K\Phi_1 \sin 2\varphi \right) \Psi = E\Psi. \tag{4.2}$$

We now introduce the quantity $q = -2K\Phi_1/\Theta$ and perform a trivial shift of the angular variable φ by defining $\theta = \varphi - \pi/4$. In terms of these new variables, the eigenvalue problem (4.2) can be written as

$$\frac{d^2\Psi}{d\theta^2} + \left(\frac{E}{\Theta} - 2q \ \cos 2\theta \right) \Psi = 0, \tag{4.3}$$

which is the well-known Mathieu equation [40]. Its eigenvalues can be labeled by a non-negative integer number m, and

for each $m \neq 0$ there are two eigenvalues: $a_m(q)$, associated with an even periodic solution, and $b_m(q)$, associated with an odd periodic solution. For $m=0$ there is just one eigenvalue $a_0(q)$ associated with an even periodic solution.

In order to find the self-consistent condition, we have to determine the order parameter

$$\Phi_1 = \langle \cos 2\theta \rangle = \frac{\Sigma_i \langle \Psi_i | \cos 2\theta | \Psi_i \rangle e^{-\beta E_i}}{\Sigma_i e^{-\beta E_i}} = \frac{1}{2} \frac{\partial f_0}{\partial q} \quad (4.4)$$

as a function of the parameter q. In Eq. (4.4) we have used the free energy per site defined as $f_0 = -(1/\beta) \ln \Sigma_i e^{-\beta E_i}$. Solving Eq. (4.4) simultaneously with the condition $q = -2K\Phi_1/\Theta$, we find the equilibrium value of the order parameter for given values of inverse temperature β and model parameters K, Θ.

Because our main interest is to determine the phase boundary and the order of the transition, we do not have to find the complete expression for $\Phi_1(q)$. For a continuous phase transition, the phase boundary is a curve in parameter space on which a nontrivial and infinitesimally small solution $\Phi_1 \neq 0$ appears, apart from the trivial one $\Phi_1 = 0$, which is always present and corresponds to the disordered phase. In order to determine the phase boundary and check the order of the transition, it is enough to find an expansion of Φ_1 in powers of q up to the third order, which can be obtained from the expansion of f_0 in powers of q up to the fourth order. The expansions of the eigenvalues of the Mathieu equation can be found in [40] and we quote here just first few of them, which have the form

$$a_0(q) = -\frac{q^2}{2} + \frac{7q^4}{128} - \cdots,$$

$$a_1(-q) = b_1(q) = 1 - q - \frac{q^2}{8} + \frac{q^3}{64} - \frac{q^4}{1536} - \cdots. \quad (4.5)$$

For practical calculations in the low-temperature region, we can truncate the infinite sum in f_0 and include only a finite number of terms. Increasing the number of terms would yield a progressively better approximation in the high-temperature limit, but this is actually not necessary, since in this limit the quantum effects become negligible and the model behaves classically. The classical model has already been investigated within various mean-field approximations in Ref. [41]. We have taken the eigenvalues corresponding to $m \leqslant 6$. The first neglected eigenvalue then equals $7^2 = 49$ for $q=0$ and therefore our approximation should yield reliable results up to temperatures that are at least an order of magnitude lower than the first neglected term, therefore for temperatures $T/\Theta \leqslant 5$. Substituting the energy eigenvalues expansions into Eq. (4.4) and calculating the free energy f_0 and order parameter Φ_1 (the actual symbolic calculation has been performed by MATHEMATICA), we find that the expansion of the latter has the form

$$\Phi_1 = \chi_1 q + \chi_3 q^3 + \cdots, \quad (4.6)$$

where the coefficients χ_1 and χ_3 are somewhat complicated expressions. Combining the expression (4.6) with the equation $q = -2K\Phi_1/\Theta$, we find that the condition for the phase boundary is given by $K_c = -\Theta/2\chi_1$. We quote here the final result for K_c, which reads

$$K_c = \frac{420\Theta_c Z_6}{420 + 210B_1[(4\Theta_c/T_c)+1] - 280B_2 - 105B_3 - 56B_4 - 35B_5 - 24B_6}, \quad (4.7)$$

where $B_m = \exp[-m^2\Theta_c/T_c]$ and $Z_6 = \Sigma_{m=-6}{}^6 B_m$.

We yet have to make sure that the transition is really continuous. The necessary and sufficient condition for this is that the coefficient χ_3 is negative on the phase boundary (4.7). We have found this to be always satisfied. Therefore the phase boundary (4.7) corresponds to a continuous phase transition. In the high-temperature classical limit this agrees with the finding in Ref. [41]. In order to map the phase diagram in the Θ^*-T^* plane, we have to set $K_c = 1$ in Eq. (4.7) and solve for T_c^* as a function of Θ_c^*. This can be done numerically and the resulting phase diagram is shown on Fig. 2.

V. RESULTS AND DISCUSSION

To start the discussion, we note that the present study of the quantum APR model was partly motivated by the strong changes in shape of the orientational order parameter Φ as a function of temperature as the rotational constant was increasing from its classical value $\Theta^* = 0$, see Fig. 3 in Ref. [22]. For small enough Θ^* it was found that the order parameter decays monotonically with increasing temperature, similarly to the classical case. This is qualitatively different for larger Θ^*, where $\Phi(T^*)$ becomes a nonmonotonic function of temperature. In the present paper, we study this regime in much more detail and vary in addition to Θ^* as well the linear dimension L of the lattice.

In Fig. 1, the order parameter vs temperature curves are shown for different system sizes and for two representative Θ^* choices: $\Theta^* = 0.6109$ in Fig. 1(a) and 0.6982 in Fig. 1(b). As can be seen from the data, in Fig. 1(a) the order parameter at low temperatures has a nonzero value and on heating first increases up to a maximum and then decreases, which means that the system develops most order at intermediate temperatures. The results obtained for different system sizes indicate that in the high-temperature region the order parameter scales to zero with increasing system size, whereas the maximum value is system size independent. Therefore, there is a long-range ordered phase at low temperatures present in addition to the disordered high-

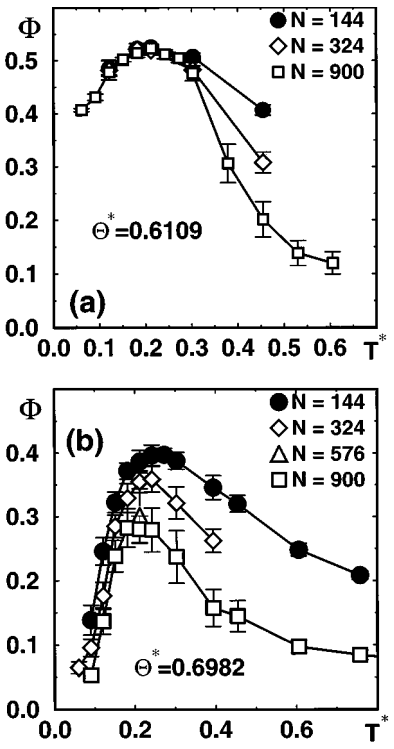

FIG. 1. Orientational order parameter Φ as a function of temperature. Symbols indicate different system sizes, statistical error bars are shown, and lines are for visual help only. The values of the rotational constants are (a) $\Theta^*=0.6109$ and (b) $\Theta^*=0.6982$.

temperature phase. This orientational ordering that takes place with decreasing temperature results in the limit $\Theta^*\to 0$ in the classical APR transition and the well-defined herringbone ordered ground state. This picture changes, however, as the quantum fluctuations get more pronounced. When the value of Θ^* is increased further, the maximum value of the long-range order parameter drops considerably with increasing system size, as can be seen for $\Theta^*=0.6982$ from Fig. 1(b). The order parameter at our lowest temperatures is now strongly depressed and also decreases further with increasing linear dimension of the system. The finite-size effects in this intermediate Θ^* range are thus pronounced not only at the high-temperature wing of the order parameter vs temperature curve, but at *all* temperatures and in particular also close to the maximum of the order parameter. This is already a hint that the residual order in this range of Θ^* values might actually be a finite-size artifact. From the previous study [22] we know that a further increase in Θ^* would suppress the ordering even more and finally lead to a situation with vanishing order parameter at any temperature. All this motivated us to analyze the behavior of the system further in order to see whether the intermediate-temperature maximum and low-temperature reduction of ordering, suggestive of a reentrant orientational melting, are really associated with the latter phenomenon. In order to answer such a question one has to employ finite-size scaling techniques that would allow us to find out whether a particular phase transition is present, and if so, to locate it.

Before we start with the numerical finite-size scaling analysis of the PIMC data, let us pause for a moment and discuss the mean-field predictions from Sec. IV. The resulting phase diagram in the Θ^*-T^* plane is shown in Fig. 2 with the solid line. We note that in the classical limiting case $\Theta^*\to 0$ we find $T_c^*=2$, which agrees with earlier mean-field calculations [41]. Any crossing of the phase boundary in the mean-field phase diagram Fig. 2 corresponds to a second-order phase transition; note that it is believed [12,5] that for $\Theta^*=0$, the classical APR model undergoes a fluctuation-driven weak first-order transition at $T^*\approx 0.76$ for $L\to\infty$. We see that at zero temperature there is a quantum phase transition at the value of $\Theta_c^{*\mathrm{MF}}=1$. The most interesting feature of the phase diagram is that there is a region of rotational constants ranging from 1 to roughly 1.25 for which the system is ordered at intermediate temperatures but disordered in the ground state (reentrance). The intuitive explanation of this phenomenon is the following. At low temperatures, the individual rotors are mostly in their totally rotationally symmetric ground state, which does not possess quadrupolar moment and therefore cannot induce ordering via the quadrupolar term. At intermediate temperatures, the excited states with nonzero quadrupolar moment become populated and induce ordering that persists to larger values of the rotational constant. According to the mean-field theory, reentrance takes place for a rather broad range of rotational constants $1<\Theta^*<1.25$. This corresponds to a decrease of the critical rotational constant by roughly 20% from its maximum value of about 1.25 to the value of 1 at the ground-state transition and represents a well-pronounced feature. Concerning the validity of this mean-field result, it is known that the mean-field approximation sometimes tends to overemphasize or even create reentrant behavior, as pointed out in Ref. [24]. On the other hand, reentrant behavior has been experimentally observed in solid HD under compression [42]. This three-dimensional system, however, although consisting of diatomic molecules interacting via approximate quadrupolar interactions, differs fundamentally from our model in spatial dimensionality and structure of the lattice as well as in the dimensionality of the order parameter. In order to settle the question of reentrance in the 2D quantum APR model, we present now the results of numerical simulations and analysis techniques.

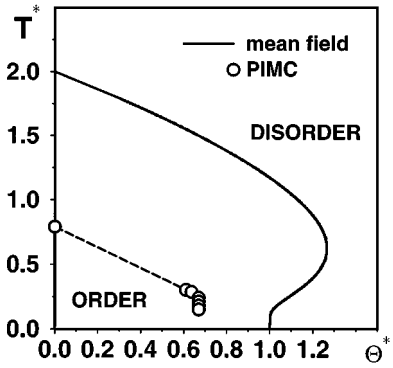

FIG. 2. Phase diagram of the quantum APR model in the Θ^*-T^* plane. The solid curve shows the line of continuous phase transitions from an ordered phase at low temperatures and small rotational constants to a disordered phase according to the mean-field approximation. The symbols show the transitions found by the finite-size scaling analysis of the path-integral Monte Carlo data. The dashed line connecting these data is for visual help only.

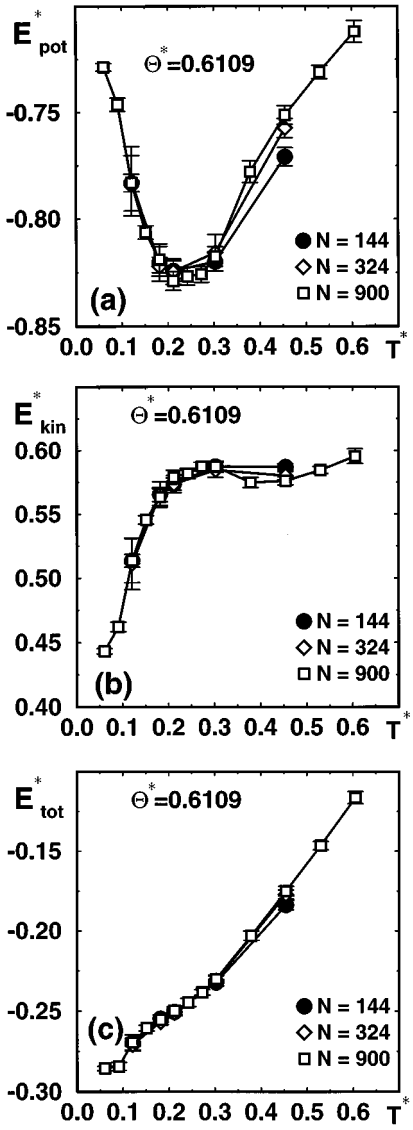

FIG. 3. Energies as a function of temperature for the rotational constant $\Theta^*=0.6109$: (a) potential energy $E_{\rm pot}$, (b) kinetic energy $E_{\rm kin}$, and (c) total energy $E_{\rm tot}$. Symbols indicate different system sizes and lines are for visual help only.

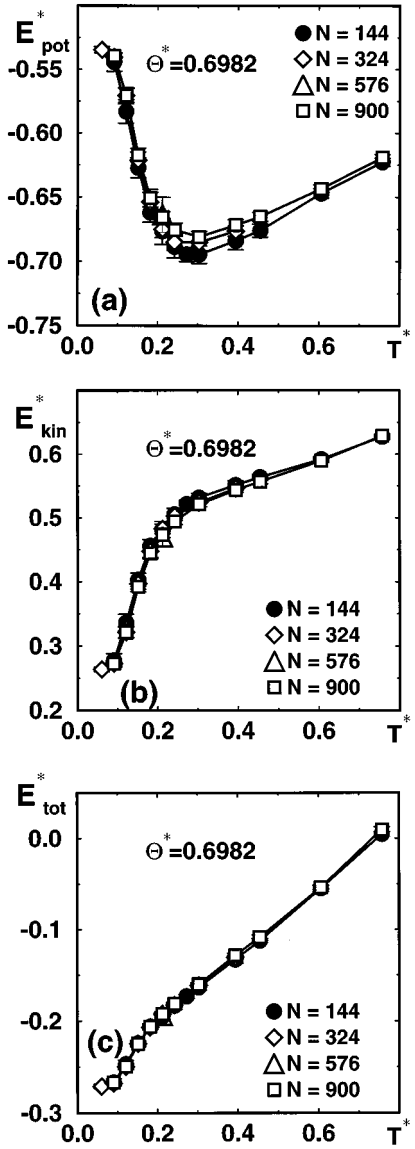

FIG. 4. Energies as a function of temperature for the rotational constant $\Theta^*=0.6982$: (a) potential energy $E_{\rm pot}$, (b) kinetic energy $E_{\rm kin}$, and (c) total energy $E_{\rm tot}$. Symbols indicate different system sizes and lines are for visual help only.

We start with the results for potential, kinetic, and total energies of our model. These are presented in Figs. 3 and 4 for two representative cases $\Theta^*=0.6109$ and $\Theta^*=0.6982$, respectively. In both cases the potential energy first decreases with temperature until maximum order is achieved, while the kinetic energy increases strongly in this region. For larger temperatures both $E_{\rm pot}$ and $E_{\rm kin}$ increase with temperature. Thus, when the temperature is increased from zero the rotators occupy higher rotational states, which allow for more pronounced orientational ordering compared to that in the ground state. In these ordered states the attractive quadrupolar interaction is larger, resulting in a lower potential energy, and the kinetic energy increases strongly with temperature due to enhanced localization of the rotators along some direction. This scenario continues with temperature until maximum order is achieved. A further increase of temperature results in an increase of $E_{\rm pot}$ due to thermal disorder, making the quadrupolar interaction less important compared to the thermal energy. This can finally lead to a phase transition from the low-temperature orientationally ordered phase to a high-temperature disordered phase, provided the rotational constant does not exceed a certain value. At very low temperatures the slope of the total energy as a function of temperature, i.e., the specific heat, approaches zero, as expected for quantum systems. We did not find a strong size dependence of $E_{\rm tot}(T^*)$ and thus the specific-heat behavior also does not seem to depend on the system size.

Similar to the total energy, the average spread R_φ, which is a measure of the quantum-mechanical delocalization of the rotators, is not dependent on system size as shown in Fig. 5. As can be seen from its definition (3.7) this quantity is a single-particle property that is by construction not particularly sensitive to collective effects. The spread approaches its classical limit, i.e., zero, for large temperatures, the approach being slower for larger Θ^*. In the limit of low temperatures, it reaches a ground-state value that is larger than 90° for the

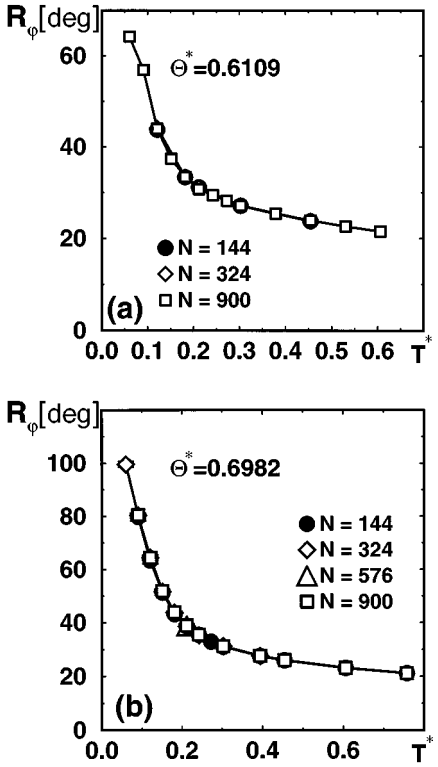

FIG. 5. Average spread R_φ in degrees as a function of temperature. The values of the rotational constants are (a) $\Theta^*=0.6109$ and (b) $\Theta^*=0.6982$. Symbols indicate different system sizes and lines are for visual help only.

rotational constant $\Theta^*=0.6982$, which means that an individual rotator is no more confined to perform librational motion around a preferred orientation, but is instead strongly delocalized. On the other hand, we know already from Fig. 1(b) that the order parameter is vanishingly small at low temperatures and decreases even more with increasing system size for this value of Θ^*. The behavior of the average spread is thus a clear demonstration that it is the quantum tunneling that induces the disordering of the ground state for sufficiently large rotational constants.

In order to finally address the question whether our system has a reentrant phase transition as predicted by the mean-field study we analyzed the low-temperature region by the cumulant intersection finite-size scaling method described in Sec. III C; see Figs. 6–8. For our smallest rotational constant $\Theta^*=0.6109$ we clearly find an intersection point for both $U_L^{(4)}$ and $U_L^{(2)}$ at about $T^*\approx 0.30$; see Figs. 6(a) and 7(a). For the larger rotational constant $\Theta^*=0.6364$ [Figs. 6(b) and 7(b)], the intersections of the fourth- and second-order cumulants occur again both at the same value within the error bars. These crossings arise because the cumulants for larger systems approach their limiting values faster than those for smaller systems. For $\Theta^*=0.6666$ the cumulants on the different length scales at low temperatures have values that cannot be distinguished within the error bars; see Figs. 6(c) and 7(c). The large value of $U^*\approx 0.65$ that was found for the classical APR model [12] causes here the problem that within our numerical accuracy we cannot identify an intersection point, but rather obtain a whole temperature region that is characterized by pronounced fluctuations. For larger Θ^* constants the behavior of the two cumulants can again be distinguished fairly well. However, contrary to what we found for $\Theta^*\leqslant 0.6364$,

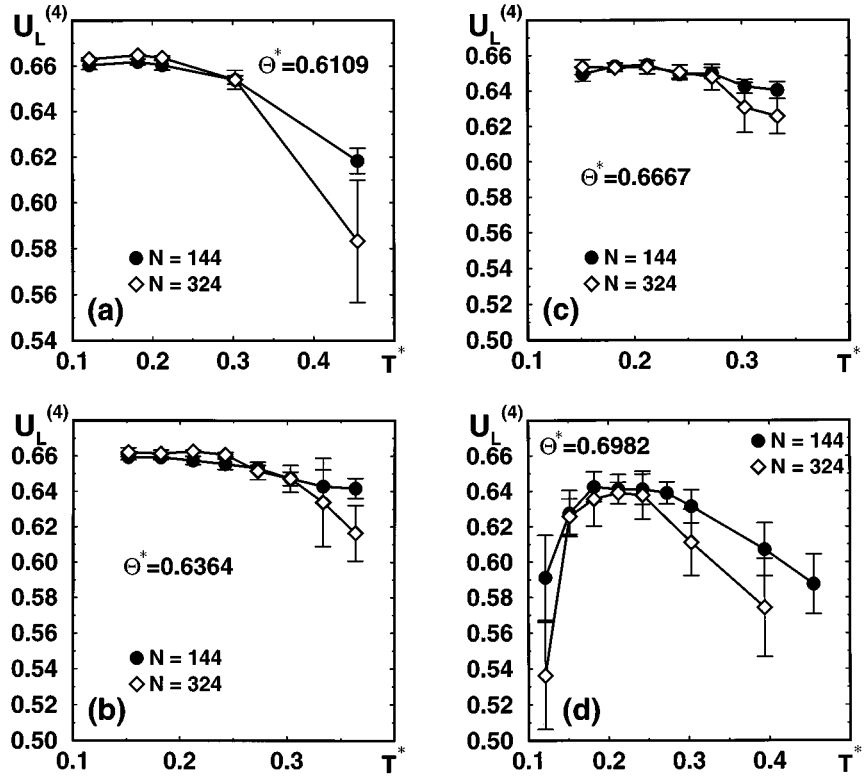

FIG. 6. Fourth-order cumulant $U_L^{(4)}$ as a function of temperature. The values of the rotational constants are (a) $\Theta^*=0.6109$, (b) $\Theta^*=0.6364$, (c) $\Theta^*=0.6667$, and (d) $\Theta^*=0.6982$. Symbols indicate different system sizes and lines are for visual help only.

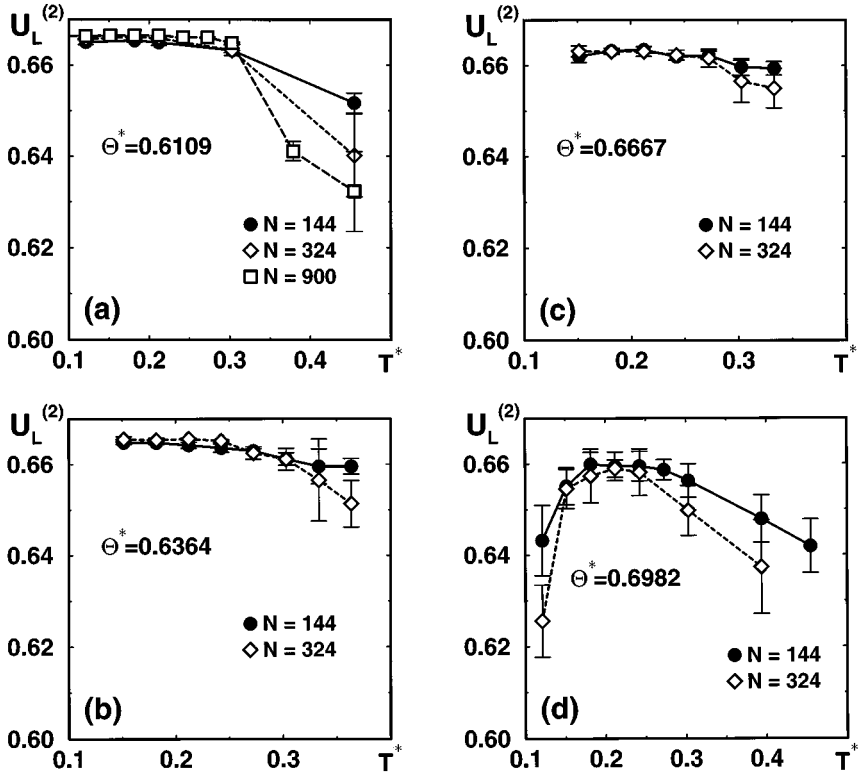

FIG. 7. Second-order cumulant $U_L^{(2)}$ as a function of temperature. The values of the rotational constants are (a) $\Theta^*=0.6109$, (b) $\Theta^*=0.6364$, (c) $\Theta^*=0.6667$, and (d) $\Theta^*=0.6982$. Symbols indicate different system sizes and lines are for visual help only.

the larger system now has the smaller cumulant throughout the whole temperature range; see Figs. 6(d) and 7(d). This signals the presence of the orientationally disordered phase for $\Theta^*=0.6982$ that extends from the ground state up to high temperatures. From this behavior of the cumulants we conclude that there is no evidence for the reentrance transition but rather a pronounced increase of short-range order at intermediate temperatures in the neighborhood of the phase boundary line. The latter has at low temperatures a roughly vertical (i.e., Θ^* independent) slope rather than the characteristic shape suggested by the mean-field result in Fig. 2.

In order to reinforce such a conclusion for this part of the phase boundary we also studied the cumulants as functions of the rotational constant at constant temperature in the range

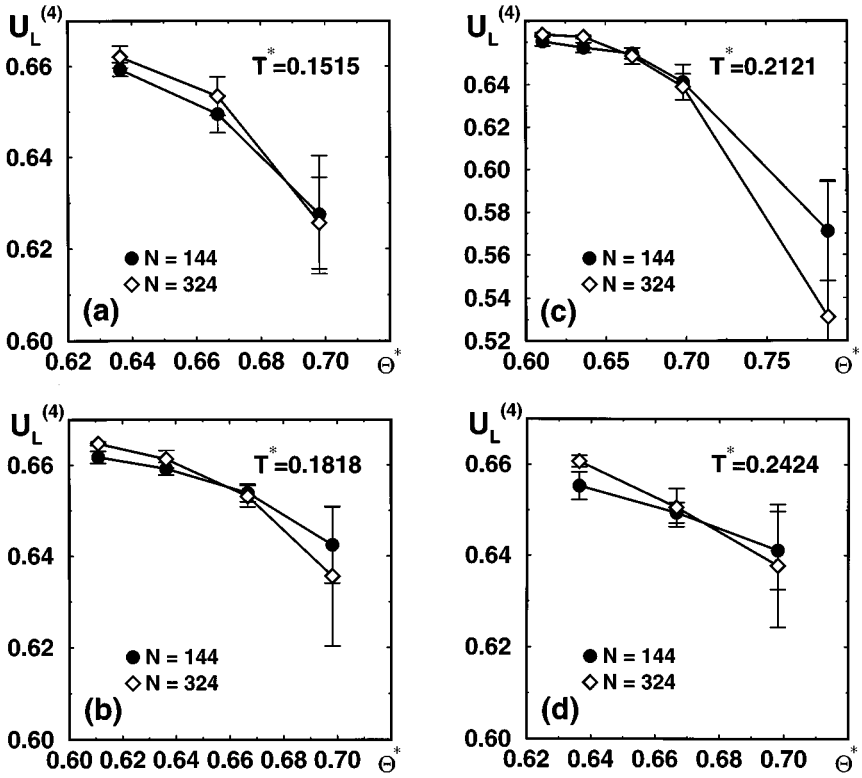

FIG. 8. Fourth-order cumulant $U_L^{(4)}$ as a function of rotational constant. The values of the temperature are (a) $T^*=0.1515$, (b) $T^*=0.1818$, (c) $T^*=0.2121$, and (d) $T^*=0.2424$. Symbols indicate different system sizes and lines are for visual help only.

$T^* \leqslant 0.2424$. The fourth-order cumulant plots of Fig. 8 show that the intersection occurs in this low-temperature range at a value of about $\Theta^* \approx 0.667 \pm 0.015$, which stays constant within the numerical noise; the second-order cumulants $U_L^{(2)}$ show the same behavior. Note that a systematic increase followed by a decrease of this quantity is expected as a function of temperature if reentrance does occur. We can furthermore infer that the nontrivial value U^* of the cumulants at crossing is also in this low-temperature regime with pronounced tunneling and quantum effects within the numerical accuracy identical to the value $U^* \approx 0.65$ found for the classical APR phase transition [12]. We are thus lead to conclude that the APR transition temperature decreases slowly from its classical limit value of $T^* \approx 0.76$ at $\Theta^* = 0$ down to about $T^* \approx 0.24$ at $\Theta^* \approx 0.67$, where it suddenly drops dramatically. This numerically obtained nonreentrant phase diagram is included in Fig. 2. The PIMC simulation results clearly exclude the existence of a strongly pronounced reentrant feature in the phase diagram. Of course, we cannot exclude the possible existence of a narrow reentrance region falling within the error bars of the present data. However, in any case these error bars are much smaller than the 20% decrease of the critical rotational constant predicted by the mean-field theory. The latter approximation is successful in predicting the phenomenon of enhanced ordering at intermediate temperatures, but the deficiency is that it exaggerates the range of order and incorrectly predicts it to become long ranged. As can be seen from Fig. 2, the mean-field theory apparently treats the quantum fluctuations (the limit $T^* \rightarrow 0$) better than the thermal fluctuations (the limit $\Theta^* \rightarrow 0$) since the transition point of the quantum-induced transition is overestimated only by a factor of about 1.5, whereas the purely classical transition is off by a factor of more than 2.

VI. SUMMARY AND CONCLUSIONS

We have studied the quantum generalization of the anisotropic-planar-rotor model consisting of point quadrupoles that are pinned with their center of rotation on a triangular lattice. This two-dimensional statistical-mechanical model system exhibits interesting orientational ordering effects, as a function of temperature and the rotational constant that controls the strength of the quantum fluctuations. A mean-field study predicts for this quantum system a reentrant orientational order-disorder transition with a pronounced reentrance region. Thus, in an intermediate range of rotational constant values at low temperatures the system orders with increasing temperature and then disorders again at higher temperatures via a phase transition, which corresponds to the well-known herringbone orientational transition in the classical limit.

We studied the quantum APR model also numerically using path-integral Monte Carlo simulations in combination with a finite-size scaling analysis in order to explore the region of the phase diagram where reentrance is expected. It turned out that no reentrant transition is present, at least within the usual numerical limitations of such simulations, which are most importantly set by the statistical errors and limited system sizes concerning both the N and P dimensionalities. In order to determine whether there still is a tiny reentrance region hidden within our numerical accuracy, at least an order of magnitude larger amount of computer time would be required, which at present seems to be prohibitively expensive. For the same reason we did not attempt to address the issue of the order of the quantum-induced APR phase transition in the ground state. We could, however, infer that the nontrivial cumulant values at the APR phase transition at low temperatures and large rotational constants are within the estimated uncertainty identical to the value obtained in the classical limit.

There are several possibilities to extend the present study. Concerning the problem of reentrance in systems consisting of quantum rotators, it might be interesting to study the effect of higher multipole interactions. In addition, it would be desirable to go beyond the mean-field approximation by means of analytical techniques, such as, renormalization techniques capable of including accurately the quantum fluctuations. Finally, it is certainly desirable to develop even more efficient quantum simulation and analysis techniques. All this demonstrates that investigations of *phase transitions* in *quantum* systems with continuous degrees of freedom are even today still a challenge.

Note added in proof. Recently, we found that the statistical error bars presented in the figures are actually larger than the true ones. The true error bars are a factor of about 3 smaller than those shown in the figures.

ACKNOWLEDGMENTS

R.M. acknowledges stimulating discussions with E. Tosatti. P.N. thanks the DFG for support (Heisenberg Foundation). We gratefully acknowledge granted computer time on the CRAY–YMP (HLRZ Jülich and RHRK Kaiserslautern) and CRAY-T90 (HLRZ Jülich) supercomputers.

[1] *Ordering in Two Dimensions*, edited by S. K. Sinha (North-Holland, Amsterdam, 1980).
[2] *Phase Transitions in Surface Films 2*, edited by H. Taub, G. Torzo, H. J. Lauter, and S. C. Fain, Jr. (Plenum, New York, 1991).
[3] *Excitations in 2-D and 3-D Quantum Fluids*, edited by A. F. G. Wyatt and H. J. Lauter (Plenum, New York, 1991).
[4] H. Wiechert, Physica B **169**, 144 (1992).
[5] D. Marx and H. Wiechert, Adv. Chem. Phys. **95**, 213 (1996).
[6] M. Kreer and P. Nielaba, in *Monte Carlo and Molecular Dynamics of Condensed Matter Systems*, edited by K. Binder and G. Ciccotti (SIF, Bologna, 1996), p. 501.
[7] S. F. O'Shea and M. L. Klein, Chem. Phys. Lett. **66**, 381 (1979); Phys. Rev. B **25**, 5882 (1982).
[8] O. G. Mouritsen and A. J. Berlinsky, Phys. Rev. Lett. **48**, 181 (1982).
[9] A. J. Berlinsky and A. B. Harris, Phys. Rev. Lett. **40**, 1579 (1978); A. B. Harris and A. J. Berlinsky, Can. J. Phys. **57**, 1852 (1979).
[10] O. G. Mouritsen, *Computer Studies of Phase Transitions and*

Critical Phenomena (Springer, Berlin, 1984).
[11] M. Schick, Surf. Sci. **125**, 94 (1983).
[12] O. Opitz, D. Marx, S. Sengupta, P. Nielaba, and K. Binder, Surf. Sci. Lett. **297**, L122 (1993); D. Marx, S. Sengupta, O. Opitz, P. Nielaba, and K. Binder, Mol. Phys. **83**, 31 (1994).
[13] A. B. Harris, O. G. Mouritsen, and A. J. Berlinsky, Can. J. Phys. **62**, 915 (1984); O. G. Mouritsen, Phys. Rev. B **32**, 1632 (1985); E. J. Nicol, C. Kallin, and A. J. Berlinsky, *ibid*. **38**, 556 (1988).
[14] H.-Y. Choi and E. J. Mele, Phys. Rev. B **40**, 3439 (1989).
[15] L. Mederos, E. Chacón, and P. Tarazona, Phys. Rev. B **42**, 8571 (1990).
[16] H.-Y. Choi, A. B. Harris, and E. J. Mele, Phys. Rev. B **40**, 3766 (1989).
[17] P. Tarazona and E. Chacón, Phys. Rev. B **39**, 7157 (1989).
[18] H. Vollmayr, Phys. Rev. B **46**, 733 (1992).
[19] D. Marx, O. Opitz, P. Nielaba, and K. Binder, Phys. Rev. Lett. **70**, 2908 (1993); D. Marx, S. Sengupta, and P. Nielaba, J. Chem. Phys. **99**, 6031 (1993).
[20] D. Marx, S. Sengupta, P. Nielaba, and K. Binder, Phys. Rev. Lett. **72**, 262 (1994); Surf. Sci. **321**, 195 (1994).
[21] D. Marx, S. Sengupta, and P. Nielaba, Ber. Bunsenges. Phys. Chem. **98**, 525 (1994).
[22] D. Marx and P. Nielaba, J. Chem. Phys. **102**, 4538 (1995).
[23] P. G. de Gennes, Solid State Commun. **1**, 132 (1963).
[24] R. M. Stratt, Phys. Rev. Lett. **55**, 1443 (1985); J. Chem. Phys. **84**, 2315 (1986).
[25] P. Fazekas, B. Mühlschlegel, and M. Schröter, Z. Phys. B **57**, 193 (1984).
[26] L. Jacobs, J. V. José, and M. A. Novotny, Phys. Rev. Lett. **53**, 2177 (1984); L. Jacobs, J. V. José, M. A. Novotny, and A. M. Goldman, Phys. Rev. B **38**, 4562 (1988).
[27] X. Wang, D. K. Campbell, and J. E. Gubernatis, Phys. Rev. B **49**, 15 485 (1994).
[28] R. Martoňák and E. Tosatti, Phys. Rev. B **49**, 12 596 (1994); E. Tosatti and R. Martoňák, Solid State Commun. **92**, 167 (1994); R. Martoňák, *Models of Quantum Paraelectric Behaviour of Perovskites* (SISSA, Trieste, 1993).
[29] B. J. Berne and D. Thirumalai, Annu. Rev. Phys. Chem. **37**, 401 (1986); M. J. Gillan, in *Computer Modelling of Fluids, Polymers and Solids*, edited by C. R. A. Catlow, S. C. Parker, and M. P. Allen (Kluwer, Dordrecht, 1990); D. Chandler, in *Liquids, Freezing and Glass Transition*, edited by J. P. Hansen, D. Levesque, and J. Zinn-Justin (Elsevier, Amsterdam, 1991); D. M. Ceperley, Rev. Mod. Phys. **67**, 279 (1995).
[30] D. Marx and P. Nielaba, Phys. Rev. A **45**, 8968 (1992).
[31] Yu. A. Freiman, V. V. Sumarokov, A. P. Brodyanskii, and A. Jezowski, J. Phys. Condens. Matter **3**, 3855 (1991); A. P. Brodyanskii, V. V. Sumarokov, Yu. A. Freiman, and A. Jezowski, Low Temp. Phys. **19**, 368 (1993).
[32] K. Binder, Z. Phys. B **43**, 119 (1981); Phys. Rev. Lett. **47**, 693 (1981).
[33] K. Binder, Ferroelectrics **73**, 43 (1987).
[34] W. K. Burton and A. H. De Borde, Nuovo Cimento **2**, 197 (1955); L. S. Schulman, *Techniques and Applications of Path Integration* (Wiley, New York, 1981); H. Kleinert, *Path Integrals in Quantum Mechanics, Statistics and Polymer Physics* (World Scientific, Singapore, 1990).
[35] D. Chandler and P. G. Wolynes, J. Chem. Phys. **74**, 4078 (1981).
[36] J. Cao, Phys. Rev. E **49**, 882 (1994).
[37] M. H. Müser, Mol. Simul. **17**, 131 (1996); M. H. Müser, B. J. Berne, Phys. Rev. Lett. **77**, 2638 (1996); D. Marx, Mol. Simul. **12**, 33 (1994); M. H. Müser, W. Helbing, P. Nielaba, and K. Binder, Phys. Rev. E **49**, 3956 (1994); K. J. Runge, M. P. Surh, C. Mailhiot, and E. L. Pollock, Phys. Rev. Lett. **69**, 3527 (1992).
[38] H. P. Deutsch, J. Stat. Phys. **67**, 1039 (1992); H. P. Deutsch and K. Binder, Macromolecules **25**, 6214 (1992).
[39] K. Vollmayr, J. D. Reger, M. Scheucher, and K. Binder, Z. Phys. B **91**, 113 (1993).
[40] *Handbook of Mathematical Functions*, edited by M. Abramowitz and I. A. Stegun (Dover, New York, 1965).
[41] E. Chacón and P. Tarazona, Phys. Rev. B **39**, 7111 (1989).
[42] F. Moshary, N. H. Chen, and I. F. Silvera, Phys. Rev. Lett. **71**, 3814 (1993).